Growth of Oriented Zinc Oxide Nanowire Array into Novel Hierarchical Structures in Aqueous Solutions

Hongxing Li,[†] Mingxia Xia,[†] Guozhang Dai,[†] Hongchun Yu,[†] Qinglin Zhang,[†] Anlian Pan,[†] Taihong Wang,[†] Yanguo Wang,*[,†,‡] and Bingsuo Zou*[,†]

Micro-Nano Technologies Research Center, Key Lab for Micro-Nano Optoeletronic Devices of MOC, Hunan University, Changsha 410082, China, and Institute of Physics, CAS, P.O. Box 603, Beijing 100080, China

Received: July 22, 2008; Revised Manuscript Received: September 5, 2008

The strategy to manipulate nanoscale building blocks into well-regulated hierarchical architectures is of great interest and valuable to both material synthesis and advanced nanodevices. Novel ZnO hierarchical structures with nanowire arrays connected on both faces of parallel ZnO hexagonal disks were produced in a facile temperature-dependent multi-step hydrothermal route within an open vessel, in which lamellar zinc hydroxide (LHS-Zn) disks were firstly formed as intermediate basic floor, whose surface may be roughened at elevated temperature; the resultant ZnO nanowires were then assembled into a highly ordered array on the top/bottom surfaces of disks in the presence of dense ammonia. Higher $[Zn^{2+}]$ at the beginning lead to multicell sandwiches or nanowire−disk−nanowire−disk−nanowire-like superlattice. Ammonia molecules in the vessel play a key role in controlling architecture evolution. Room-temperature Raman-scattering and photoluminescence measurements indicated the optical properties of single as-prepared ZnO structure.

1. Introduction

Nanostructures with controlled architectures are desirable for many potential applications due to their physical and chemical properties which are determined by morphology, size, and dimensions.[1−3] Stepwise oriented attachment and aggregation of large number of nanoparticles in three dimensions has been widely reported during monocrystalline organization or biomineralization.[4,5] It involves spontaneous self-assembly of adjoining particles in cases where particles are free to move, by rotating with respect to each other so that they may share a common crystallographic orientation. The growth and aggregation behaviors of the particles can be influenced by selective adsorption of organic ligands on different crystalloid interfaces due to the anisotropic adsorption affinity.[6,7] Inorganic materials usually can be organized into exceptional shape and size through organic and inorganic cooperative interaction at the inorganic−organic interface. Crystal materials such as ZnO nanorods/boxes/disks/rings,[8−10] CuO ellipsoids,[11] and Fe_3O_4 nanospheres/sheets[12,13] have been synthesized by this mechanism.

ZnO is an important wide band-gap (3.37 eV at room temperature) semiconductor with a large exciton binding energy (60 meV).[14] As a versatile, mutifunctional material, it has been extensively used in several industrial products, such as white paints, ceramics, food additives, catalysts, electronic materials, spintronics, and boimedical applications.[15] For spintronics devices, homostructures with nanowire or nanodots in between are usually needed to preserve the carrier coherency between two or more poles, while nanodots often have large scattering sites. Hence, the structure of bulk−nanowire−bulk−nanowire−bulk are especially useful. However, no-defect bulk−nanowire connections in other techniques are seldom realized. In order to obtain a different nano-shaped ZnO structure, various physical and chemical fabrication techniques including thermal evaporation, metal−organic chemical vapor deposition(MOCVD), laser ablation, and colloidal wetting chemical synthesis have been developed to synthesize ZnO nanostructures. A wide range of morphologies of ZnO nanostructures such as nanowires,[16] nanobelts,[17] nanosprings,[18] and nanotubes,[19] and more others have been synthesized, and they showed novel electronic, optical, mechanical, and sensing properties.[11−13] Along with the one-dimensional structures, systematic shape-controlled syntheses of the hierarchical ZnO nanostructures are emerging as new challenges in the researches of ZnO nanosystems. By using high temperature vapor−liquid−solid (VLS) growth process, novel ZnO morphologies such as hierarchical heteronanostructures,[20] nanopropeller arrays,[21] nanobridges,[22] and multi-forked structures[23] have been demonstrated. In contrast to the VLS approaches, solution routes are particularly attractive because of their potential for low-temperature/cost and industrial mass manufacturing. Branched complex ZnO nanostructures formed in solution mainly follow a single reaction stage or multiple steps. On the basis of this technique, flowerlike,[24] treelike arrays,[25] and dandelion[26] structures have been synthesized by one-pot hierarchical organizing process. By nucleating new oriented nanocrystals on crystals or structures formed in a prestage, oriented arrays of rod or needle-shaped ZnO crystals grow on the core rods has been reached by Zhang et al.[27]

In this paper, we tried to utilize mixed zinc nitrate solution and over-amounted strong ammonia as precursors to react in a open vessel at elevated temperature. We obtained hexagonal disks of brucite-type polynuclear zinc hydroxyl at first, then nanowires on them by self-oriented attachment of nanoclusters, and evaporating NH_3 molecules and water in their alkaline aqueous solutions at slightly lower temperature. Finally ZnO-bundled nanowire arrays anchored to {0001} top/bottom ocean planes were produced based on such hexagonal disks by a multistep growth process. The resultant nanocomplexes are pure in compostion, and the 6-fold-symmetry matches well with the disk shape. The approach is simple, low cost, and product

* To whom correspondence should be addressed. E-mail: ygwang@blem.ac.cn (Y.W.); bszou@hnu.cn (B.Z.).
† Hunan University.
‡ Institute of Physics.

10.1021/jp806677q CCC: $40.75
Published on Web 10/21/2008

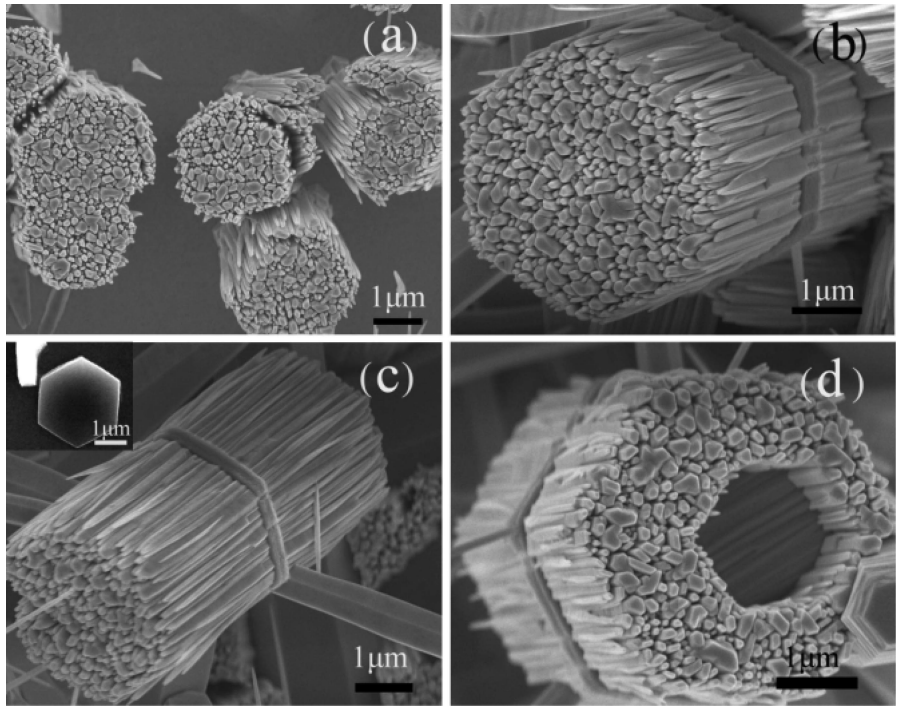

Figure 1. SEM images of the hexagonal disk based bundled ZnO. (a) The top view of the bundles standing on the substrate. (b and c) Nanowire bundles grown from the two widest surfaces of the disk. (The inset of c shows the disk obtained before the secondary nanowire growth). (d) Overall view of a individual hollow hierarchical architecture.

oriented. As compared with previous reports on ZnO nanotip arrays growing into "nanotips-rod" geometry, ZnO nanonails, or rotorlike ZnO hierarchical nanostructures from a mixture of rodlike ZnO powder and a saturated $Zn(OH)_4^{2-}$ solution under moderate hydrothermal conditions; this formation of hexagonal-disk-based ZnO hierarchical nanostructures possess novel configurations. The organization processes has been studied, which may be used for the growth mechanism of other materials. Due to the quantum confinement nature of nanowires and superlattice character, this configuration may be used to study the confined exciton or carrier transport via nanowire between the bulk disks, which may be important in the future spintronics and luminescence properties and applications.

2. Experimental Section

2.1. Sample Preparations. In a typical synthetic process, Zinc nitrate hexahydrate ($Zn(NO_3)_2 \cdot 6H_2O$, 98+%, Shanghai) and ammonium hydroxide of analytical reagent grade purchased from commercial sources (NH_4OH, 25−28 wt % in water, 99.99%) were used directly as zinc cation and hydroxide anion precursors in pure water, respectively. No further purification of these chemical reagents was made, and also no other additive reagents were used in this synthesis. The precursor solutions were made by dissolving 2.8 mmol of $Zn(NO_3)_2 \cdot 6H_2O$ into 5 mL of pure water (18 MΩ) under magnetic stirring using a 60 mL crucible (with lid) as a container, and then 40 mL of ammonia reagent was slowly added; the mixed solution was continuously stirred for several minutes at room temperature, and pieces of cleaned ITO plates with a size of 1 cm × 1 cm were placed into the crucible with the conducting face up (step 1). The mixed solution in the crucible (transparent) was kept open at a constant temperature of 95 °C for about 10 h (step 2) and then was slowly cooled at 0.75 °C/min down to 40 °C and kept open at this temperature for about 20 min (step 3). At that point, the whole volume decreased to less than 70% of the original. At that time, the solution became turbid. Then the solution temperature was elevated to 100 °C and kept at 100 °C for another 30 min (step 4). After this step the final products formed on the surface of ITO plates. The whole volume of the final solution was left to about 60% for the evaporating process. After being washed with absolute ethanol and distilled water, the plates were dried in the air at 70 °C overnight. Only increasing the concentration of $Zn(NO_3)_2 \cdot 6H_2O$ from 2.8 to 3.0 mmol at the beginning with no other change in conditions gave the product.

2.2. Sample Characterizations. The phase structures of as-synthesized products were identified using powder X-ray diffraction (XRD, Siemens D-5000 diffractometer with Cu Kα (λ = 1.5418 Å)). The morphology, size, and structure of the products on ITO substrate were characterized by field-emission scanning electron microscopy (JEOL SEM 6700F) with energy-dispersive X-ray spectroscopy and a transmission electron micriscope (JEOL 2010) operated at 200 kV. Room-temperature photoluminescence was detected by using a commercial near-field scanning optical microscopy (NSOM). A focused He−Cd laser (325 nm) as the excitation source was illuminated on a single ZnO bundled hierarchical structure, and the emitted light was collected into a double monochromator. A chromatic color CCD through an objective lens was used to collect the far-field topography and optical image. Raman spectra were recorded using a Raman spectroscope (alpha SNOM 3000S) with an Ar^+-ion laser at 488 nm.

3. Results and Discussion

3.1. Morphologies, Structures, and Growth Processes. Zinc oxide hierarchical structures with nanowire bundles originated from both the top and bottom surfaces of a hexagonal disk were prepared in an aqueous solutions by using multistep hydrothermal synthesis method in an open beaker. The hexagonal disks were found to work as the intermediate products. A large number of hexagonal disks based ZnO nanowire bundled structures were finally found on the conducting surface of ITO

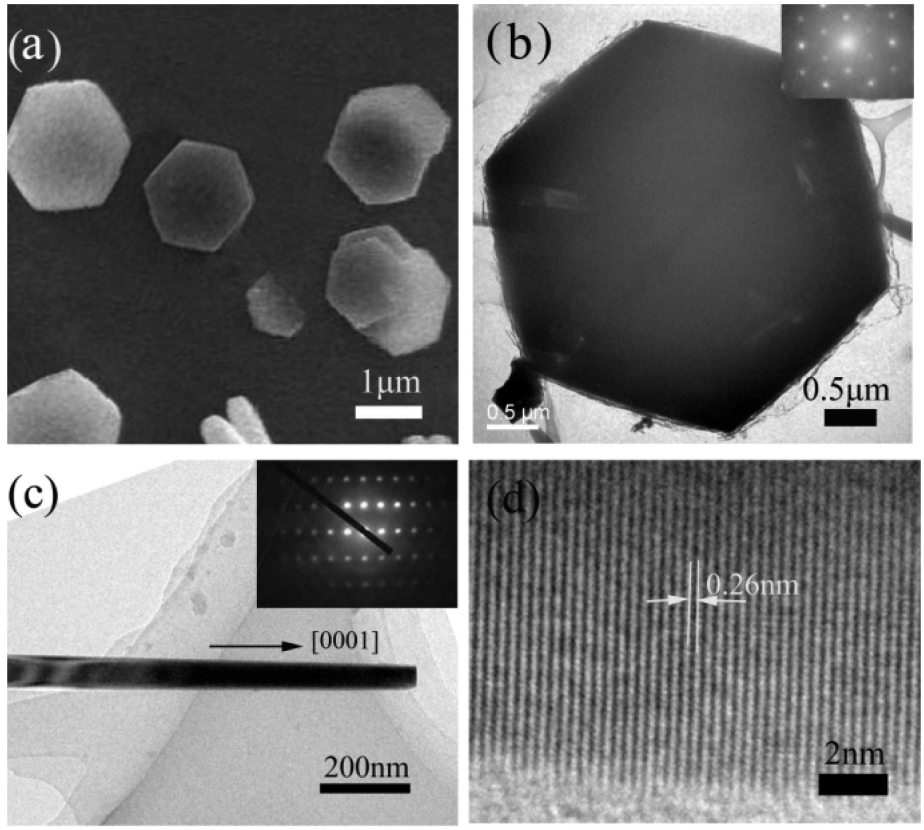

Figure 2. SEM image (a) and low-magnification TEM image (b) of the ZnO hexagonal disks before nanowire growth. A corresponding SEAD pattern is shown in the inset of (b). (c) TEM image of single ZnO nanowire and the SAED pattern (inset). (d) Corresponding HREM image.

substrate (Figure 1). This novel structure consists of a hexagonal large disk and nanowire arrays epitaxialy grown from the {0001} planes of the disk. Each bundle preserves a fairly good facet structure which matches well to the 6-fold-symmetric disk substrate, as if they are a single entity of a large hexagonal column. Each individual nanowire in the bundle is clearly identified and has almost the same growth rate so that the 6-fold-symmetric nanowire bundled structure is preserved on the disks. Sometimes we also found some hollow bundled structures lying on the substrate (Figure 1d). Careful examination indicates that the hollow space of the big disk contains another small disk edge in which nanowires may grow up (see the Supporting Information, Figure S-1). The small disk may stand perpendicularly to the surface of the big one for charge matching, the different growth rate of nanowires on these two disks, and spatial blocking effect caused such morphology. Compositional examination by energy-dispersive X-ray spectrometer (EDX) indicated that the bundled structures are only composed of Zn and O (Zn/O = 49.4:50.6), no other impurities (inset of Figure 2) existed.

To understand the growth processes of such hierarchically organized ZnO microstructures, the intermediate microstructures at different growth stages were identified by monitoring their nanostructure evolutions. After heating the crucible for 10 h at 95 °C, only minor nanorods sparsely spread over the surface of the ITO plates (see the Supporting Information, Figure S-2) and the solution volume decreased to 70%. This may be the product of ZnO crystals caused by the reaction between $Zn(NH_3)_4^{2+}$ complex and hydroxyl OH^-, but dominant Zn should exist with complex ions. Figure 2a indicates after 20 min of reacting at 40 °C, a large amount of regular hexagonal disks on the ITO substrate have been observed. These perfect hexagonal disks show a sub-micrometer thickness with layered characteristics for some cracks between layers are clearly present on the hexagonal sides. The disk in solution can turn into ZnO after a suitable thermal treatment at about 100 °C (Figure 2b). The TEM image of the nanowire on the surface of disk (final product) is shown in Figure 2c and d, which is discussed later. During the nourishing time, the solution become turbid with dispersed sol particles, which can precipitate at a time of hours. The particles can also be cathodically electrodeposited onto the ITO surface with separate nanosheet arrays, as shown in Figure 3a. Its XRD results (Figure 3c) identify it as $Zn_5(OH)_8(NO_3)_2 \cdot 2H_2O$ (JCPDS Card No. 25-1028). All the disks stand up on the ITO surface with side-edge connecting ITO plate, which reflected that the charges at side-edge of disk are positive. When the ITO plate carrying $Zn_5(OH)_8(NO_3)_2 \cdot 2H_2O$ disks are heated in air at 200−300 °C for an hour, pores formed on the up-face and down-face of the disk (Figure 3b). The pored disks is ZnO by XRD verification with significant weight loss. This indicates that the disks underwent a reorganization and decomposition process and gas leaking out of its surface during annealing, which left the nanofluctuated surface. Clearly, such a heating-induced process can also happen when the $Zn_5(OH)_8(NO_3)_2 \cdot 2H_2O$ disks are suspended in the ammonia solution,[28,29] although it may not be thorough.

The experiments revealed that lowering the reaction temperature from 95 to 40 °C (step3) is indispensable to the formation of disklike zinc hydroxynitrate. When the mixed solution was elevated to 100 °C immediately after step 2, there are no hexagonal disks obtained on the ITO plate but only enlarged rodlike crystals formed like that formed at 95 °C. From the literature,[28,29] layered hydroxide zinc salt nanostructures can be obtained by alkaline reaction at a temperature in the range of 30−60 °C, ZnO was only produced when the reaction temperature was above 70 °C. Notably, these hexagonal disks are quite

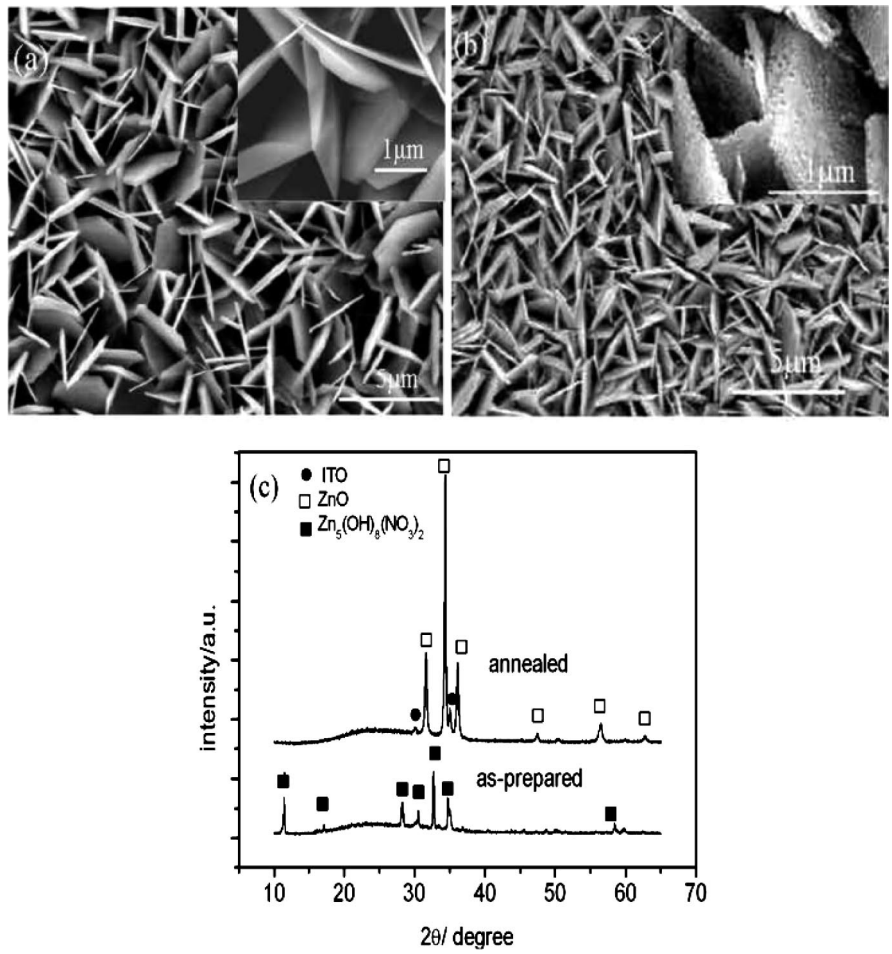

Figure 3. SEM images of the sample on the ITO glass obtained by electrodeposition before (a) and after (b) annealing (inset is magnified). (c) XRD patterns of the sample on ITO before and after annealing.

distinctive from previously reported lamellar zinc hydroxynitrate, which were composed of thin crumpled sheets without any definite shape, owing to the turbostratic disorder.[30,31] That these nanoparticle composed aggregates would organize together to form crystal layers has been widely reported for the crystal growth and biomineralization.[32−34] Indeed, metal ions such as Cu^{2+}, Zn^{2+}, Co^{2+}, and Ni^{2+} form the initial kinetic phases of layered hydroxide metal nitrates (LHS-M; M = copper, zinc, cobalt, and nickel) under hydrothermal conditions in an alkaline medium, which are easy to crystallize in the slablike shape because of its layered crystallographic structure.[31,35−37] The layer slab LHS-Zn is composed of zinc hydroxide tetrahedral ZnO_4 and octahedral ZnO_6, with NO_3^- anions intercalated the positively charged layers of the hydroxide $[Zn_5(OH)_8(H_2O)_2]^{2+}$ to keep charge neutrality. By dehydration, these metal hydroxynitrates transform into the corresponding metal oxides and preserve their lamellar character with varied surface. We also checked the $ZnCl_2$ solution as precusors; similar results were obtained.

The detailed texture and crystal orientation of the first-formed disk were further investigated by TEM. Before TEM observation, the products were dried in the air at 80 °C for several hours. Figure 2b shows the overview of a hexagonal disk at low magnification. The inset SAED pattern can be indexed to the hexagonal wurtzite structure of zinc oxide along the [0001] zone axis. However, careful observation indicated that some disk surface was coated by a layer of amorphous spongelike nano laces (Figure S-3a). An unfledged hexagonal disk architecture was also investigated by TEM; the corresponding HRTEM image proves that the unfledged disk is porous in nature and appears to be an fluctuated distribution of many nanoparticles on the surface (Figure S-3b). This clearly is the solution effect, the surface of crystal often contain some amorphous layers. The *d* spacing between adjacent lattice planes among these nanoparticle is 0.248 nm, coincident with the space between (0−110) planes in ZnO (see the Supporting Information, Figure S-3c). This result indicates that LHS-Zn transformation into ZnO occurs easily at a slightly high temperature.

The last growth process happened in an open vessel at boiling temperature, the preformed disk gradually transformed into ZnO in the core structure after decomposition, and many nano-islands on its up and down surfaces were left. Then further growth occured on the fluctuated peaks on the disk surface for a lot of available nanoclusters ($Zn(OH)_4^{2-}$). The islands should be the initial site for the nanowire growth. Because the islands are almost uniformly distributed on the smooth face of the disk, the nanowire bundle form based on these islands collectively. HRTEM for Individual nanostructures confirm that the nanowires among the bundle are single-crystalline and grow along the [0001] direction (Figure 2c). The lattice fringe of about 0.26 nm in Figure 2d corresponds to the (0002) lattice spacing. Moreover, all of the nanowires in one bundle were observed to be originated from the same basal surface of hexagonal disk (see the Supporting Information, Figure S-4).

As an important anion-exchange material,[28,31,38] LHS-Zn consists of a stacking of brucite-type polynuclear zinc hydroxyl layers. When the reaction temperature is elevated in the presence of ammonia, thermally induced nucleation burst-out on the

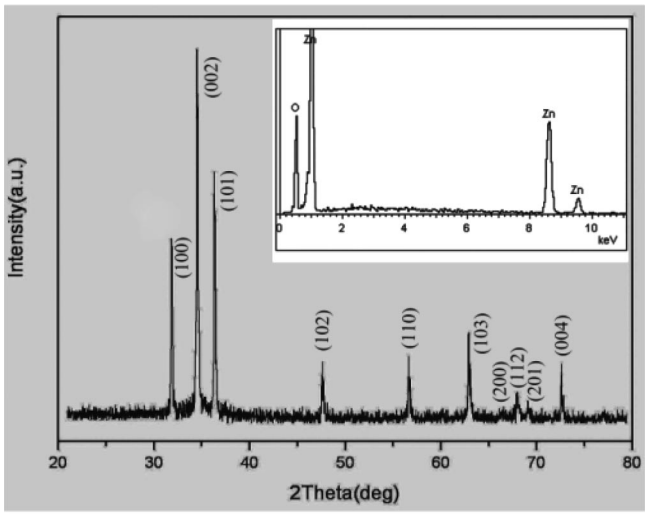

Figure 4. XRD pattern of ZnO products. All peaks can be attributed to the pure wurtzite phase of ZnO. EDX (inset) of the disk-based ZnO structures.

surface layer and lead LHS-Zn transformation to ZnO. The disk morphology and crystal structure of LHS-Zn, which include the [001] activity for ZnO growth from the anisotropic packing force of $Zn(OH)_x$ unit and interplay with the exchanges between NH_3 and OH^- in the surface zinc hydroxide layer, lead to the preservation of the original morphology.[28,29] Zinc cations of polynuclear zinc hydroxyl units are reserved in their original positions to minimize the change of the Gibbs free energy for thermodynamic stability during the thermal decomposition. This would lead to the formation of ZnO nanoparticle islands on the surface of the original disk at elevated temperature. NH_3 may act as a promotive and etching agents in this process[10] which etch the smooth surface of $Zn(OH)_x$ and blocked the interconnection of nanoparticles. Thereafter, ZnO islands, as a template, would adsorb $Zn(OH)_4^{2-}$ preferentially on and grow along the <0001> direction owing to its crystal habit, lead to high-quality vertical ZnO nanowire arrays like that reported in using (110) facet of Al_2O_3,[39,40] (001) facet of GaN,[41] or *c* oriented ZnO thin film[42] as a nanowire nucleation layer. This ZnO nanowire array is believed to be grown epitaxially on these substrate, in which the effect of ammonia is indispensable. The final-product structure is different from our hexagonal disk with regular nanosized pits on its up and down surfaces formed at the early stage. Therefore, the growth mechanism of this disk-based ZnO nanowire array is different than those reported previously.

It is interesing that nanowire growth seldom occurs at the side-edge of a disk. Three factors may be involved. (1) The preferential growth direction is along the *c* axis. (2) The charge effect at the side-edge did not support alkaline spcies growth; neutral location should be the favorate site for dehydration growth. (3) The decomposed or etched location in the central can supply more $Zn(OH)_x$ species than the side-edge for further growth. Detailed discussions are listed in the next section.

The crystal structures were further investigated by X-ray diffraction (XRD). Figure 4 demonstrates XRD pattern for the as-synthesized final products. All diffraction peaks can be indexed to the pure wurtzite phase of ZnO (JCPDS Card No. 89-1397). The enhanced (0002) reflection may originate from the large numbers of ZnO nanowire bundled structures were perpendicular to the substrate, as shown in the SEM image (Figure 1a).

The morphology of the disk-based ZnO hierarchical structure can also be modified by adjusting the amount of initial substances. Dramatically, when increasing the amount of $Zn(NO_3)_2 \cdot 6H_2O$ from 2.8 to 3.0 mmol in the beginning, sandwich structures with wire bundles-disks iteratively formed in the final products. Figure 5a−d shows low-magnification SEM images, while Figure 5e and f shows the higher-magnification SEM images across the parallel flakes. Figure 5g shows the top view of this unique structure, in which most of nanowires with flat top standing perpendicularly to the surface of disk. Thick disks before the secondary nanowire growth turn into bilayerd even multilayerd architectures as shown in Figure 5h−i, their diastemas in the multilayered disks can be seen clearly. Therefore, well-defined by this special slitted slabs, zinc-hydroxyl complexes ($Zn(OH)_4^{2-}$) and NH_3 can be supposed to diffuse into the in-between region, taking part in the concurrent etching and growth processes, and lead to the array/disk/array/disk/array sandwich structures in last nanowire growth step. Before nanowire growth, this type of disks is more like the cycle conjugated molecules, which may form a H-aggregate with intermolecular interaction at suitable concentration. Such interaction may be dimished by the edge charge, which may leave space for small species to get into.

Due to the growth model,[10,43] the disks have higher defect density at the up central region and larger charge density at the edges and corners, which lead to an decreasing of binding energy for the incorporation of external molecules from center to corner. The surface defects at the central region of the disk are often considered to be reactive with the release of NH_4^+ and NH_3 and result in local etching. The higher the temperature, the faster the etching action.[10] Careful examination indicated that after the secondary or nanowire growth step, the thickness of disks (after step 4) (with nanowire grown at up and down surface) become thinner than the disks before nanowire growth (step 3). This is caused by the selective local surface dissolution near the local defects on the polar plane {0001} of the disk into the solution at elevated temperature, which makes the in-between nanowire growth more quickly and easier. At the same time, some residual fragments on the nanowire surface at the mesosphere of the sandwich structures can be clearly observed because larger charge density at the disk edges and corners (side-edge) slow down the dissolving rate at the lateral surfaces. All nanowire assembles are found in the central area of the disk surface; no wire was observed at the edges and side faces. Furthermore, the nanowires in between disks are shorter in length than that in both ends. Of course the *c* axis growth for disk is the dominant factor when the above charge spatial effect takes effect. Other factors like aqueous solution growth with ammonia, fast removing of gaseous species, water evaporating from solid at high temperature, and strain induced by the phase transformation may also facilitate the sandwiched nanowire array growth.

3.2. Growth Mechanism and Reactions. On the basis of the above experiment and observation, the self-oriented attachment and sequential hierarchical growth mechanism are depicted as follows. With adding excess ammonia into the zinc nitrate aqueous solution, zinc ions form the amine complex ($Zn(NH_3)_4^{2+}$);[44] at this moment no ZnO forms at any temperatures. When the temperature of the solution elevates, a lot of NH_3 evaporates. Then the alkaline environment take effect at reducing temperature. Hence, the $Zn(NH_3)_4^{2+}$ complexs begin hydrolysis and pyrolysis to form the special nuclei seeds (disks). Then the bundled ZnO nanowires form on the surface of disk. The chemical reactions in these processes are suggestd below.

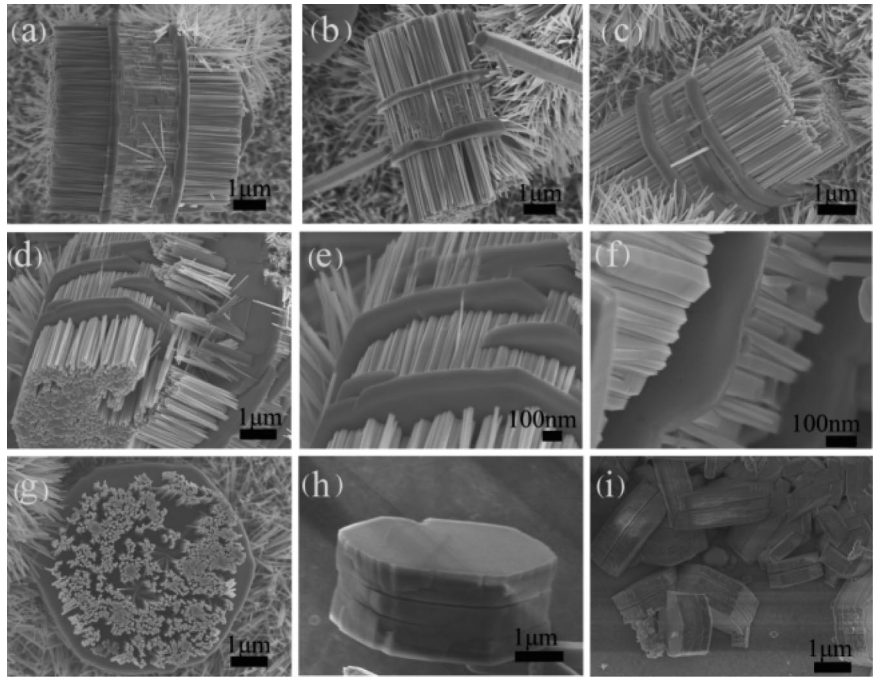

Figure 5. (a−f) SEM images of the sandwich structures. (g) Top view with nanowires standing standing perpendicularly to the surface of the disk. (h−i) Multilayer diastema disk structures before nanowire growth.

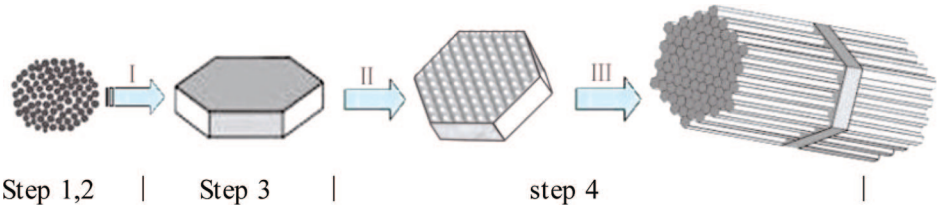

Figure 6. Schematic illustration of the formation of hexagonal disk based ZnO hierarchical structures: (I) Self-oriented aggregation of small particles into hexagonal disk of LHS-Zn. (II) Nucleation site generation caused by transformation of LHS-Zn into ZnO. (III) The sequential growth of the nanowire array.

Step 1:

$$Zn(NO_3)_2 + 4NH_3 \cdot H_2O \rightarrow Zn(NH_3)_4(NO_3)_2 + 4H_2O \quad (1)$$

Step 2: remove excess NH_3 by heating,

$$Zn(NH_3)_4^{2+} + 4OH^- \rightarrow Zn(OH)_4^{2-}(aq) + 4NH_3\uparrow \quad (2)$$

Step 3: reducing temperature,

$$3Zn(NH_3)_4^{2+} + 2Zn(OH)_4^{2-} + 2NO_3^- + 14H_2O \rightarrow Zn_5(OH)_8(NO_3)_2 \cdot 2H_2O\downarrow + 12NH_3 \cdot H_2O \quad (3)$$

Step 4: increasing temperature

$$Zn_5(OH)_8(NO_3)_2 \cdot 2H_2O + 4NH_3 \cdot H_2O \xrightarrow{\Delta} 4ZnO(s)\downarrow + 10H_2O\uparrow + Zn(NH_3)_4(NO_3)_2(aq) \quad (4)$$

$$(NH_3)_4Zn_2(OH)_4 \xrightarrow{\Delta} 2ZnO(s)\downarrow + 4NH3\uparrow + 2H_2O \quad (5)$$

In a hydrothermal reaction, small metal hydroxide nanoclusters usually aggregate and grow into rodlike structures in alkaline solutions at high temperature, as reported in the literature.[45] However, if lowering the solution temperature after a period of heating, the step 3 is the formation of hexagonal disks $Zn_5(OH)_8(NO_3)_2 \cdot 2H_2O$ (in reaction 3),[43,46] which worked as the template for next growth. This disk is mainly composed of metastable hydroxide with hexagonal shape and can transform into ZnO (reaction 4) at high temperature. In this transformation many regular nanosized pits were left on the surface of the hexagonal disk after water crystalized off with the assistance of ammonia. The formation of these pits is due to in situ decomposition with H_2O boiloff out of the disk surface mildly with the occurrence of NH_3 coordination. Hence, the disk surface possesses many regular peaks of ZnO islands left for next nanowire growth. At the moment of this decomposition, the concurrent $Zn(NH_3)_4^{2+}$ complex (reaction 4) could be released then transform into $Zn(OH)_4^{2-}$ to join onto these ZnO peaks for the parallel nanowire growth.

The whole formation process of the ZnO hierarchical structure is schematically illustrated in Figure 6. The critical step is step 3, which leads to the formation of hexagoanl disk. Excess NH_3 and OH^- will not produce disk at high temperature for coordinated complex. Open-air steps 2 and 4 led NH_3 and H_2O to evaporate partially at boiling point, and facilitated the ZnO formation. The possible role of amine groups passivate on the metal oxide surface have been discussed by Zhang et.al,[27] who suggested the varied amount of amine groups adsorbed on different surface planes might depend on the corresponding surface density of metal atoms. In contrast to the above case of passivation, ammonia molecules play a role in etching the $Zn_5(OH)_8(NO_3)_2 \cdot 2H_2O$ disk (reaction 4) in our growth and facilitate the formation of ZnO nanowire (reaction 5). Due to the mild conditions, the surface of disk can be dissolved

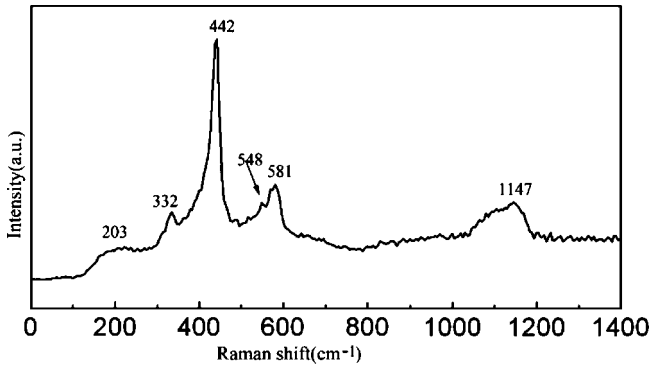

Figure 7. Room-temperature Raman spectrum of the ZnO products.

gradually into the island array for second ZnO nanowire growth. A revived in situ aggregation driving force along the *c* axis comes from the intrinsic growth impetus of the ZnO crystal, which favors the nanowire formation along the *c* axis in the next step.

What is the effect of ITO plate? In preformed disks the charges of the hexagonal disk are mainly distributed on the edges, so the disk can be easily adsorbed on the surface of ITO conducting face with the side-standing (see Figure 3a).[43] This configuration facilitates the later nanowire growth and protects the disk aggregation. Of course there are some exceptions. Due to the ammonia location and concentration effect, it is possible to see two disks standing much closer and more parallel, which may cause misoriented aggregation and intergrowth during the second nanocrystal generation.[5] The hollow bundled structures, therefore, can also be obtained in the step 4. In the second nanowire growth, increasing reaction temperature or keeping the reaction solution at boiling is important for the hierarchical growth, while ITO plate play a role to adsorb disks and reduce the collision and aggregation between disks.

3.3. Room-Temperature Raman and Photoluminescence Properties of Single ZnO Hierarchical Structure. Room-temperature Raman spectra were recorded using a Raman spectroscope with the Ar^+-ion laser at 488 nm served as the excitation source. ZnO with wurtzite structure belongs to the C_{6v}^4 space group. At the Γ point of the Brillouin zone, optical phonons have the following irreducible representation: $\Gamma_{opt} = A_1 + 2B_1 + E_1 + 2E_2$.[47] Among these, A_1 and E_1 modes are polar and can be split into transverse (TO) and longitudinal optical (LO) components, with all being Raman and infrared active. For the sample, vibration peaks can be clearly observed at 203, 332, 442, 548, 581, and 1147 cm^{-1} (Figure 7). Among these peaks, the strongest one centered at about 442 cm^{-1} is characteristic of the high-frequency E_2 mode of the wurtzite structure. The peak at 548 and 581 cm^{-1} correspond to the LO phonon of A_1 and E_1, respectively. Besides these "classical" Raman modes, the Raman spectra also show other modes with frequencies of 203, 332, and 1147 cm^{-1}. These additional peaks cannot be explained within the framework of the bulk single phonon modes, which are attributed to the multiphonon scattering processes, which is usully enhanced in the 1-d nanowires.[48]

The PL from the single ZnO hierarchical structure consists of a clear UV emission around 380 nm and a visible emission band centered at around 556 nm range from 450 to 750 nm (Figure 8). The visible emission usually unavoidable for ZnO in air, in which at least three emission peaks can been seen clearly, a strong peak at 556 nm and two shoulders at 483 and 657 nm. It is well known that visible luminescence in ZnO mainly originates from surface defect states such as Zn

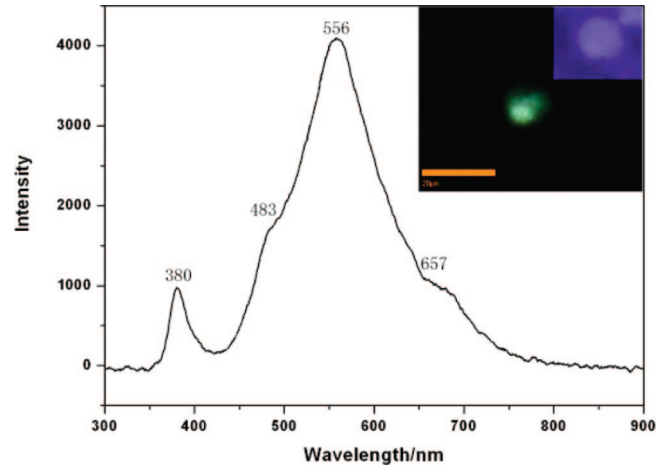

Figure 8. Room-temperature photoluminescence spectra of the single ZnO hierarchical structure. (inset) Far-field PL image and corresponding bright-field topography.

interstitials and oxygen vacancies.[49,50] Moreover, the product by hydrothermal reaction usually gives green emission for much surface defects. Here the green emission peak around 556 nm is extra sharp and high. The local visible light emission of these ZnO hierarchical structure under CW laser excitation of 325 nm was so strong that it could be imaged easily with a color CCD camera and the green luminescence was visible to the naked eye in dark field (inset of Figure 8). The UV emission is usually attributed to recombination of free excitons, for near band-edge emission, which can be seen in the spectra easily. The emission often happens at the end of nanowires,[51] which reflected the 1-d advantage for collective emission. The as-observed ultraviolet emission is important for application in laser devices or display devices because the 1-d optical cavity effect can lead to lasing efficiency. Well defined by the hexagonal family floor with superlattice strucutre, on which the nanowires have the same length, crystallography orientation and close packed each other and constitute a nanowire array matrix. Such structure may also work as the transistor target for the spintronic and nanoelectronic study, because the excitons and carriers passing nanowire may be controlled to keep their coherence. Under the focused laser beam pumped or electric pumped on the disk part, each nanowire may act as a luminescence emission end, so that the coherent luminescence emission from the nanowire matrix would be greatly enhanced, which is under further studys.

4. Conclusion

We demonstrated a simple temperature-controlled multistep open hydrothermal synthesis route to obtain orientation-controlled ZnO hierarchical structures. By controlling the primary crystal shape and location of sequential growth of nanowire, bundled nanowires grown on ZnO hexagonal disks can be obtained. The Zn^{2+} concentrations and etching action of NH_3H_2O play important roles in controlling the morphology and structure of the preformed $Zn_5(OH)_8(NO_3)_2$ microdisks and thereby determining the subsequent hierarchical assembly processes and the eventual ZnO structures with nanowire bundles. Clear UV optical emission and multiphonon scattering from ZnO nanostructures has been observed, which favored the collective effect. This work may provide a rational approach to the collective behaviors in the growth of nanowire array on the substrate of same compound using the intrinsic growth habits. To our understanding, this highly ordered structure represents

an ideal candidate for photon collectors, photoelectric converter, laser, catalysts, and electronic applications.

Acknowledgment. The authors are grateful to the financial support of the NSFC of China (No.90606001, 60571044, 10774174) and 973 National Key Basic Research program of MOST of China (2002CB713802, 2007CB310500).

Supporting Information Available: SEM images of the hollow hierarchical structure, nanorods; TEM, HRTEM, and enlarged high-resolution TEM images of an unfledged hexagonal disk; TEM image of the bundled nanowires root to the basal. This material is available free of charge via the Internet at http://pubs.acs.org.

References and Notes

(1) Sounart, T. L.; Liu, J.; Voigt, J. A.; Hsu, J. W. P.; Spoerke, E. D.; Tian, Z. R.; Jiang, Y. B. *Adv. Funct. Mater.* **2006**, *16*, 335–344.
(2) Zhang, J.; Sun, L.; Yin, J.; Su, H.; Liao, C.; Yan, C. *Chem. Mater.* **2002**, *14*, 4172–4177.
(3) Xia, Y.; Yang, P.; Sun, Y.; Wu, Y.; Mayers, B.; Gates, B.; Yin, Y.; Kim, F.; Yan, H. *Adv. Mater.* **2003**, *15*, 353–389.
(4) Peen, R. L.; Banfield, J. F. *Science* **1998**, *281*, 969–971.
(5) Peen, R. L. *J. Phys. Chem. B* **2004**, *108*, 12707–12712.
(6) Tian, Z. R.; Voigt, J.; Liu, J.; Mckezie, B.; Mcdermott, M. J.; Rodrguez, M.; Konishi, H.; Xu, H. F. *Nat. Mater.* **2003**, *2*, 821–826.
(7) Peng, Y.; Xu, A. W.; Deng, B.; Antonietti, M.; Colfen, H. *J. Phys. Chem. B* **2006**, *110*, 2988–2993.
(8) Goldberger, J.; Sirbuly, D. J.; Law, M.; Yang, P. *J. Phys. Chem. B* **2005**, *109*, 9–14.
(9) Zhao, F. H.; Lin, W. J.; Wu, M. M.; Xu, N. S.; Yang, X. F.; Tian, Z.; Su, Q. *Inorg. Chem.* **2006**, *45*, 3256–3260.
(10) Li, F.; Ding, Y.; Gao, P.; Xin, X. Q.; Wang, Z. L. *Angew. Chem.* **2004**, *116*, 5350–5354.
(11) Kind, H.; Yan, H. Q.; Messer, B.; Law, M.; Yang, P. D. *Adv. Mater.* **2002**, *14*, 158–160.
(12) Jia, B. P.; Gao, L. *J. Phys. Chem. C* **2008**, *112*, 666–671.
(13) Chin, K. C.; Chong, G. L.; Poh, C. K.; Van, L. H.; Sow, C. H.; Lin, J.; Wee, A. T. S. *J. Phys. Chem. C* **2008**, *112*, 1851–1856.
(14) Wan, Q.; Li, Q. H.; Chen, Y. J.; Wang, T. H.; He, X. L.; Li, J. P.; Lin, C. L. *Appl. Phys. Lett.* **2004**, *84*, 3654–3656.
(15) Huang, M.; Mao, S.; Feick, H.; Yan, H.; Wu, Y.; Cho, H. J.; Yang, P. *Science* **2001**, *292*, 1987–1899.
(16) Huang, M. H.; Wu, Y.; Feick, H.; Tran, N.; Weber, E.; Yang, P. *Adv. Mater.* **2001**, *13*, 113–116.
(17) Pan, Z. W.; Dai, Z. R.; Wang, Z. L. *Science* **2001**, *291*, 1947–1949.
(18) 18Kong, X. Y.; Ding, Y.; Yang, R. S.; Wang, Z. L. *Science* **2004**, *303*, 1348–1351.
(19) Yu, H. D.; Zhang, Z. P.; Han, M. Y.; Hao, X. T.; Zhu, F. R. *J. Am. Chem. Soc.* **2005**, *127*, 2378–2379.
(20) Lao, J. Y.; Wen, J. G.; Ren, Z. F. *Nano. Lett.* **2002**, *2*, 1287–1291.
(21) Lao, J. Y.; Huang, J. Y.; Wang, D. Z.; Ren, Z. F. *Nano. Lett.* **2003**, *3*, 235–238.
(22) Gao, P. X.; Wang, Z. L. *Appl. Phys. Lett.* **2004**, *84*, 2883–2885.
(23) Han, X. H.; Wang, G. Z.; Zhou, L.; Hou, J. G. *Chem. Commun.* **2006**, 212–214.
(24) Pan, A. L.; Yu, R. C.; Xie, S. S.; Zhang, Z. B.; Jin, C.; Zou, B. S. *J. Cryst. Growth* **2005**, *282*, 165–172.
(25) Zhao, F. H.; Li, X. Y.; Zheng, J. G.; Yang, X. F.; Zhao, F. L.; Wong, K. S.; Wang, J.; Lin, W. J.; Wu, M. M.; Su, Q *Chem. Mater.* **2008**, *20*, 1197–1199.
(26) Liu, B.; Zeng, H. C. *J. Am. Chem. Soc.* **2004**, *126*, 16744–16746.
(27) Zhang, T. R.; Dong, W. J.; Keeter-Brewer, M.; Konar, S.; Njabon, R. N.; Tian, Z. R. *J. Am. Chem. Soc.* **2006**, *128*, 10960–10968.
(28) Song, R. Q.; Xu, A. W.; Deng, B.; Li, Q.; Chen, G. Y. *Adv. Funct. Mater.* **2007**, *17*, 296–306.
(29) Gui, Z.; Liu, J.; Wang, Z.; Song, L.; Hu, Y.; Fan, W.; Chen, D. *J. Phys. Chem. B* **2005**, *109*, 1113–1117.
(30) Hosono, E.; Fujihara, S.; Kimura, T.; Imai, H. *J. Colloid Interface Sci.* **2004**, *272*, 391–398.
(31) Poul, L.; Jouini, N.; Fievet, F. *Chem. Mater.* **2000**, *12*, 3123–3132.
(32) Li, Y.; Tan, B.; Wu, Y. *Chem. Mater.* **2008**, *20*, 567–576.
(33) Pacholski, C.; Kornowski, A.; Weller, H. *Angew. Chem., Int. Ed.* **2002**, *41*, 1188–1191.
(34) Rajam, S.; Mann, S. *J. Chem. Soc., Chem. Commun.* **1990**, 1789.
(35) Zhao, F.; Lin, W.; Wu, M.; Xu, N.; Yang, X.; Tian, R.; Su, Q *Inorg. Chem.* **2006**, *45*, 3256–3260.
(36) Jayan, B. R.; Rosa, E.; Guzman, S.; Rodriguez, R.; Yacaman, M. *J. Phys. Chem. C* **2008**, *112*, 240–246.
(37) Zhang, H.; Zhu, Q.; Zhang, Y.; Zhao, L.; Yu, B. *Adv. Funct. Mater.* **2007**, *17*, 2766–2771.
(38) Meyn, M.; Beneke, K.; Lagaly, G. *Inorg, Chem.* **1993**, *32*, 1209–1215.
(39) Huang, M. H.; Mao, S.; Feick, H.; Yan, H.; Wu, Y. Y.; Kind, H.; Weber, E.; Russo, R.; Yang, P. *Science* **2001**, *292*, 1897–1899.
(40) He, J. H.; Lao, C. S.; Chen, L. J.; Davidovic, D.; Wang, Z. L. *J. Am. Chem. Soc.* **2005**, *127*, 16376–16377.
(41) Yan, M.; Zhang, H. T.; Widjaja, E. J.; Chang, R. P. H. *J. Appl. Phys.* **2003**, *94*, 5240–5246.
(42) 42Greene, L. E.; Law, M.; Tan, D. H.; Montano, M.; Goldberger, J.; Somorjai, G.; Yang, P. *Nano. Lett.* **2005**, *5*, 1231–1236.
(43) Wang, F. F.; Li, R. B.; Pan, A. L.; Cao, L.; Cheng, K.; Xue, B. F.; Wang, G.; Meng, Q. B.; Li, J. H.; Li, Q.; Wang, Y. G.; Wang, T. H.; Zou, B. S. *Mater. Lett.* **2007**, *61*, 2000–2003.
(44) Yamada, A.; Miyazaki, H.; Chiba, Y.; Konagai, M. *Thin Solid Films* **2005**, 480–481.
(45) Li, Y. G.; Tan, B.; Wu, Y. Y. *Chem. Mater.* **2008**, *20*, 567–576.
(46) Schwenzer, B.; Roth, K. M.; Gomm, J. R.; Murr, M.; Morse, D. E. *J. Mater. Chem.* **2006**, *16*, 401–407.
(47) Decremps, F.; Porres, J. P.; Saitta, A. M.; Chervin, J. C.; Polian, A. *Phys. Rev. B* **2002**, *65*, 092101−092104.
(48) Liu, R. B.; Pan, A. L.; Fan, H. M.; Wang, F. F.; Shen, Z. X; Yang, G. Z.; Xie, S. S.; Zou, B. *J. Phys.: Condens. Matter* **2007**, *19*, 136206–136207.
(49) Zhang, S.B.; Wei, S. H.; Zunger, A. *Phys. Rew. B* **2001**, *63*, 075205−075301.
(50) Vanheusden, K.; Seager, C. H.; Warren, W. L.; Tallant, D. R.; Voigt, J. A. *Appl. Phys. Lett.* **1996**, *68*, 403–405.
(51) Wang, F.f.; Cao, L.; Pan, A.L.; Liu, R.b.; Wang, X; Zhu, X.; Wang, S.q.; Zou, B.S. *J. Phys. Chem. C* **2007**, *111*, 7655.

JP806677Q